

Resolving the degeneracy in top quark Yukawa coupling with Higgs pair production

Gang Li,^{1,*} Ling-Xiao Xu,^{2,†} Bin Yan,^{3,‡} and C.-P. Yuan^{3,§}

¹*Department of Physics, National Taiwan University, Taipei, Taiwan 10617*

²*Department of Physics and State Key Laboratory of Nuclear Physics and Technology, Peking University, Beijing 100871, China*

³*Department of Physics and Astronomy, Michigan State University, East Lansing, MI 48824, USA*

The top quark Yukawa coupling (y_t) can be modified by two dimension-six operators \mathcal{O}_H and \mathcal{O}_y with the corresponding Wilson coefficients c_H and c_y , whose individual contribution cannot be distinguished by measuring y_t alone. However, such a degeneracy can be resolved with Higgs boson pair production. In this work we explore the potential of resolving the degeneracy of the unknown Wilson coefficients c_H and c_y at the 14 TeV LHC and the 100 TeV hadron colliders. Combining the information of the single Higgs production, $t\bar{t}h$ associated production and Higgs pair production, the individual contribution of c_H and c_y to y_t can be separated. Regardless of the value of c_H , the Higgs pair production can give a strong constraint on c_y at the 100 TeV hadron collider. We further show that it is possible to differentiate various c_y and c_t values predicted in several benchmark models.

Introduction. Top quark Yukawa coupling (y_t) is the only coupling with the magnitude of order one in the Standard Model (SM). As the largest Yukawa coupling, it is important for vacuum stability and cosmology [1, 2]. Besides, in many new physics (NP) scenarios [3–7], top quark plays an important role in triggering the electroweak symmetry breaking (EWSB) and is directly connected to new physics beyond the SM. Therefore, it is highly motivated to understand the top quark Yukawa sector better, both theoretically and experimentally. The parameter y_t can be measured directly by the $t\bar{t}h$ associated production. Recently, this process is confirmed by both the ATLAS and CMS collaborations with signal strengths $\mu_{t\bar{t}h} = 1.32^{+0.28}_{-0.26}$ and $1.26^{+0.31}_{-0.26}$ [8, 9], respectively, at the Large Hadron Collider (LHC) with $\sqrt{s} = 13$ TeV. Besides, y_t can also be measured in loop-induced single Higgs boson production [10, 11], $t(\bar{t})hj$ associated production [12] and multi-top production processes [13, 14]. With higher luminosity being accumulated, one expects the accuracy on y_t can be further improved. It is thus timely to study what kind of NP can modify y_t .

In general, we can parameterize NP effects on y_t by several higher dimensional operators in a model independent way. Out of the complete set of dimension-6 operators listed in Ref. [15], we consider in this work the two operators which can modify y_t at tree level:

$$\mathcal{L} = \mathcal{L}_{\text{SM}} + c_H \mathcal{O}_H + (c_y \mathcal{O}_y + \text{h.c.}) + \dots \quad (1)$$

in the so called Strongly-Interacting Light Higgs (SILH) basis [16, 17], where the dimension-six operators

$$\begin{aligned} \mathcal{O}_H &= \frac{1}{2v^2} \partial^\mu (H^\dagger H) \partial_\mu (H^\dagger H), \\ \mathcal{O}_y &= -\frac{y_t^{\text{SM}}}{v^2} H^\dagger H \bar{Q}_L \tilde{H} t_R. \end{aligned} \quad (2)$$

Here, c_H and c_y are the corresponding Wilson coefficients with c_y being assumed to be real, Q_L is the left-handed

third-family quark doublet, $v = 246$ GeV is the vacuum expectation value, $y_t^{\text{SM}} = m_t/v$ is the SM top Yukawa coupling, and m_t is the top quark mass. As \mathcal{O}_H modifies the Higgs boson wave function, it can universally shift all the single Higgs couplings, hence, affects y_t .

Theoretically, the operators \mathcal{O}_H and \mathcal{O}_y can be induced by several different NP scenarios. For example, scalar singlets interacting with the Higgs doublet can induce the universal \mathcal{O}_H operator [18–22], while additional vector-like fermions can induce the operator \mathcal{O}_y via mixing with the top quark [23, 24]. As both the operators in Eq. (2) can induce deviations in y_t , one cannot differentiate their individual contributions if we only measure the top Yukawa coupling. Even if y_t is measured to be consistent with the SM prediction, one cannot exclude the possibility of having cancellation among different NP operators. Or, if the deviation in y_t is established, we still need to separate the effects of \mathcal{O}_H and \mathcal{O}_y for better understanding the origin of NP. Since the effect of the \mathcal{O}_H operator is to simply rescale any amplitude involving a single Higgs boson by a factor $1/\sqrt{1+c_H}$ after renormalizing the Higgs boson field, its effect is universal and can be measured from studying the hVV ($V = W^\pm, Z$) couplings. However as shown in Ref. [25], in case that Higgs boson is a pseudo Nambu-Goldstone boson, other operator (at the order of $\mathcal{O}(p^2)$) can mimic the effect induced by \mathcal{O}_H on hVV couplings. Hence, it requires novel method to separately measure the coefficients of those two types of operators [25]. Likewise, in this work, we explore the possibility of separately measuring the coefficients of \mathcal{O}_H and \mathcal{O}_y , both contributing to top Yukawa coupling y_t , through Higgs boson pair production $gg \rightarrow hh$. In addition to modifying the single Higgs effective coupling of $ht\bar{t}$, both \mathcal{O}_H and \mathcal{O}_y can also contribute to the effective coupling $hht\bar{t}$, but with different combinations, which can be measured via Higgs boson pair production. Namely, studying Higgs boson pair production can be utilized not only for measuring

Higgs self interactions, but also for discriminating new physics scenarios in the top sector. Only after the individual contribution of each effective operator is extracted can we further solidify the SM or otherwise establish NP models.

Higgs boson pair production. The gluon-initiated Higgs pair production can be used to measure the trilinear Higgs self-coupling [26–47]. It is also sensitive to various NP models [20, 21, 48–55]. After the EWSB, the effective Lagrangian related to the non-resonant Higgs pair production is [56–61]

$$\mathcal{L}_h = -\frac{m_h^2}{2v}c_3h^3 - \frac{m_t}{v}c_t\bar{t}th - \frac{m_t}{v^2}c_{2t}\bar{t}th^2 + \frac{\alpha_s c_g}{12\pi v}hG_{\mu\nu}^a G_a^{\mu\nu} + \frac{\alpha_s c_g}{24\pi v^2}h^2 G_{\mu\nu}^a G_a^{\mu\nu}, \quad (3)$$

where a is the color index, $\alpha_s = g_s^2/4\pi$ with g_s being the strong coupling strength, and m_h is the Higgs boson mass. The SM, at tree level, corresponds to $c_3 = c_t = 1$ and $c_{2t} = c_g = 0$. Then the squared amplitude of $gg \rightarrow hh$, after averaging over the gluon polarizations and colors, is [61]

$$|\overline{\mathcal{M}}|^2 = \frac{\alpha_s^2 \hat{s}^2}{256\pi^2 v^4} \left[\left| \frac{3m_h^2}{\hat{s} - m_h^2} c_3 \left(c_t F_\Delta + \frac{2}{3} c_g \right) + 2c_{2t} F_\Delta + c_t^2 F_\square + \frac{2}{3} c_g \right|^2 + |c_t^2 G_\square|^2 \right], \quad (4)$$

where $F_\Delta \equiv F_\Delta(\hat{s}, \hat{t}, m_h^2, m_t^2)$, $F_\square \equiv F_\square(\hat{s}, \hat{t}, m_h^2, m_t^2)$ and $G_\square \equiv G_\square(\hat{s}, \hat{t}, m_h^2, m_t^2)$ are the form factors [62] with \hat{s} and \hat{t} being the canonical Mandelstam variables. The first term inside the bracket contributes to s -wave and the G_\square term to d -wave component whose contribution to total cross section is numerically negligible [63].

To avoid any momentum dependent contributions to the Higgs self couplings induced by \mathcal{O}_H , we adopt the generalized canonical normalization of the Higgs field and perform the field redefinition [59, 64]:

$$h \rightarrow \frac{h}{\sqrt{1+c_H}} - \frac{c_H h^2}{2(1+c_H)^2 v}, \quad m_t \rightarrow \frac{m_t}{1 + \frac{1}{2}c_y}. \quad (5)$$

Applying this shift of the Higgs field throughout the Standard Model Lagrangian \mathcal{L}_{SM} leads to multiple Higgs couplings to any pair of massive gauge bosons or massive fermions. The effective couplings c_t and c_{2t} are derived as

$$c_t = \frac{2+3c_y}{\sqrt{1+c_H}(2+c_y)}, \quad c_{2t} = \frac{c_H(3c_y-2)+6c_y}{2(c_H+1)^2(c_y+2)}. \quad (6)$$

We note that c_t and c_{2t} have different dependence on the Wilson coefficients c_H and c_y . Also, $c_t = 1 - c_H/2 + c_y$ and $c_{2t} = 3c_y/2 - c_H/2$, when $c_y, c_H \ll 1$ [59, 60].

In Fig. 1 the dependence of c_t and c_{2t} on c_H and c_y is shown. It is clear that the slope of c_{2t} (dashed lines) is different from c_t (solid lines), especially when $c_{2t} < 0$ and $c_t < 1$. Precise study on the effective coupling c_{2t}

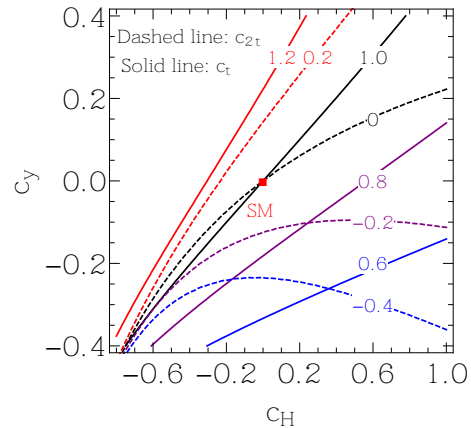


FIG. 1. The contours of c_t (solid lines) and c_{2t} (dashed lines) in the plane of c_H and c_y . The number on each curve denotes the specific value of the Higgs effective coupling c_t or c_{2t} .

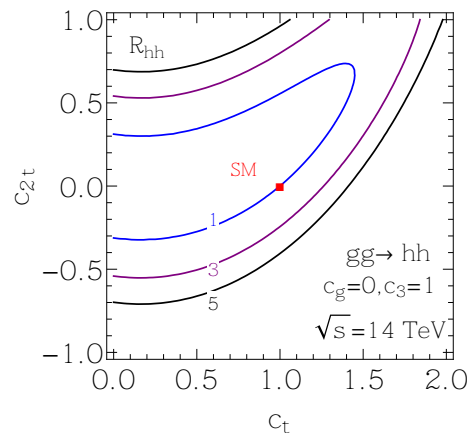


FIG. 2. The contours of R_{hh} in the plane of c_t and c_{2t} , with $c_g = 0$ and $c_3 = 1$, at the 14 TeV LHC. The red box denotes the SM values ($c_t = 1$, $c_{2t} = 0$).

therefore offers the possibility to discriminate the effects of c_H and c_y .

As shown in Eqs. (3) and (4), c_3 and c_g also contribute to the Higgs pair production cross section. However, c_g is already constrained to be within c_g^- and c_g^+ by the signal strength measurements of single Higgs production $gg \rightarrow h$ [10, 11]

$$c_g^\pm = \frac{3}{2} \left(-c_t F_\Delta \pm \sqrt{R_h} |F_\Delta| \right), \quad (7)$$

where $R_h \equiv \sigma(gg \rightarrow h)/\sigma^{\text{SM}}(gg \rightarrow h)$, the sign “ \pm ” refers to the cases $c_t F_\Delta > -2/3c_g$ and $c_t F_\Delta < -2/3c_g$, respectively. The combined fit to the single Higgs production, which depends on both c_t and c_g [56], and decay using 13 TeV LHC data gives rise to $R_h = 1.07 \pm 0.09$ (ATLAS [10]) and $R_h = 1.23 \pm 0.13$ (CMS [11]). By fixing R_h , we can replace c_g with a function of c_t . Further-

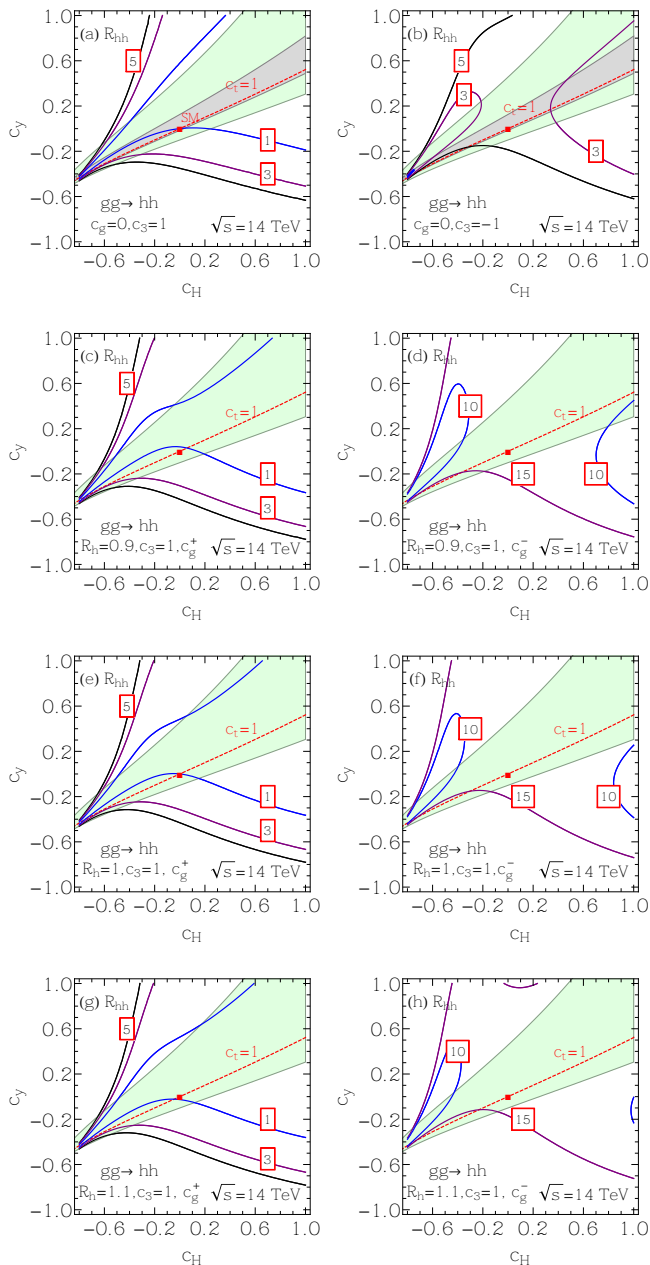


FIG. 3. The contours of R_{hh} in the plane of c_H and c_y at the 14 TeV LHC. The green and gray bands correspond to the constraints, at the 2σ C.L., from the measurements of $t\bar{t}h$ and single Higgs production cross section, respectively, at the 13 TeV LHC. The red box denotes $(c_H = 0, c_y = 0)$, while the red dashed line denotes $c_t = 1$. c_g^\pm refers to the sign choices “ \pm ” in Eq. (7) with R_h being fit from single Higgs production and decay data.

more, the coupling c_3 in Eq. (3) is approximately equal to $1 - \frac{3}{2}c_H + c_6$, as shown in Refs. [59, 60], and is weakly constrained, $-5.0 < c_3 < 12.1$, by present data [65, 66]. Here, c_6 is the coefficient of the dimension-6 operator $\mathcal{O}_6 = \lambda/v^2|H|^6$. As the Higgs pair production cross sec-

tion is more sensitive to the sign of c_3 , rather than its magnitude [67], we will choose $c_3 = \pm 1$ as our benchmark value in the following numerical analysis.

To compare $\sigma(gg \rightarrow hh)$ with the SM prediction, we define a ratio R_{hh} as

$$R_{hh} = \frac{\sigma(gg \rightarrow hh)}{\sigma^{\text{SM}}(gg \rightarrow hh)}. \quad (8)$$

In Fig. 2, we show the contours of R_{hh} at the 14 TeV LHC in the plane of c_t and c_{2t} , with other parameters chosen as $c_g = 0$ and $c_3 = 1$. R_{hh} can be enhanced largely for both the positive and negative c_{2t} , but R_{hh} is more sensitive to negative c_{2t} when c_t is of order one, which can be understood with Eq. (4). In the large top quark mass limit, $F_\Delta \rightarrow 2/3$ and $F_\square \rightarrow -2/3$ [62]. Besides, the $c_t^2 F_\square$ term dominates over the $c_t F_\Delta$ term for $c_t \gtrsim 1$. Therefore, a negative c_{2t} can enhance R_{hh} more easily than a positive c_{2t} , for this choice of c_g and c_3 [57].

With the information from Figs. 1 and 2, we conclude that it is hopeful to discriminate the effects of c_H and c_y through Higgs pair production, especially for the negative c_{2t} region. Furthermore, we could translate the above results in the plane of (c_H, c_y) . In Fig. 3, we show the contours of R_{hh} with respect to the Wilson coefficients c_H and c_y , where various choices of the effective couplings c_g and c_3 are considered. They correspond to

- (a) $c_g = 0, c_3 = 1$; (b) $c_g = 0, c_3 = -1$;
- (c) $R_h = 0.9, c_3 = 1, c_g^+$; (d) $R_h = 0.9, c_3 = 1, c_g^-$;
- (e) $R_h = 1, c_3 = 1, c_g^+$; (f) $R_h = 1, c_3 = 1, c_g^-$;
- (g) $R_h = 1.1, c_3 = 1, c_g^+$; (h) $R_h = 1.1, c_3 = 1, c_g^-$. (9)

For the cases (a) and (b), the hgg effective coupling c_g is assumed to vanish while the trilinear Higgs self-coupling c_3 is assumed to be +1 and -1, respectively. In these cases, we include the constraints on the parameter space of c_H and c_y from the single Higgs production [10, 11]; cf. the gray band of Fig. 3 (a, b). It amounts to $c_t = 1.03 \pm 0.04$ (ATLAS) and $c_t = 1.11 \pm 0.06$ (CMS). For the cases from (c) to (h), c_g is derived from a given R_h value, cf. Eq. (7), while c_3 is fixed to be identical to the SM value. For comparison, we also show the parameter space constrained by the $t\bar{t}h$ measurements at the 13 TeV LHC, with an integrated luminosity of 79.8 fb^{-1} from ATLAS [8] and of 35.9 fb^{-1} from CMS [9]. Here, we take the combined best fit $t\bar{t}h$ signal strength normalized to the SM prediction, such that $c_t = 1.15_{-0.11}^{+0.12}$ (ATLAS) and $c_t = 1.12_{-0.12}^{+0.14}$ (CMS).

With the result depicted in Fig. 3, several comments are in order:

- R_{hh} is enhanced in some parameter space of c_H and c_y , the magnitude of the enhancement strongly depends on the choice of c_3 and c_g .

- In case (b), the cancellation between the triangle diagram and box diagram does not happen, because of the negative c_3 which further enhances R_{hh} [30].
- In case of c_g^+ or c_g^- , the value of c_g is extracted from the signal strength of single Higgs production process R_h . We find that the variation of $R_h = 0.9, 1$, or 1.1 can only slightly change the value of R_{hh} .
- R_{hh} is more sensitive to c_g^- than c_g^+ . According to Eq. (7), c_g^+ is close to zero for a positive c_t , and accordingly the contours of R_{hh} are similar to the contours in case (a). On the other hand, negative c_g^- can significantly deviate from zero and R_{hh} is largely enhanced (cf. Eq. (4)).
- In cases (a), (c), (e) and (g), the possible enhancement of R_{hh} can only come from the deviations of c_t and c_{2t} . With the information of Figs. 1 and 2, R_{hh} can be largely enhanced when $c_{2t} < 0$, which corresponds to the region $c_y < 0$ in Fig. 3.

Sensitivity at the 14 TeV LHC and the 100 TeV hadron collider. Now we discuss the potential of discriminating the Wilson coefficients c_H and c_y at the 14 TeV LHC and the 100 TeV proton-proton hadron collider. As a concrete example, we examine the $b\bar{b}\gamma\gamma$ channel, which has been studied by the ATLAS collaboration at the High-Luminosity LHC (HL-LHC), operating at the center-of-mass energy of 14 TeV with an integrated luminosity of 3 ab^{-1} [68]. As being discussed in Refs. [56, 57], an analytical function can be used to describe the fraction of signal events passing through the kinematic cuts. Since the Higgs boson is a scalar particle and the $gg \rightarrow hh$ process is dominated by the s -wave contribution, the acceptance of the kinematic cuts, in the inclusive Higgs pair production, will mainly depend on the invariant mass of the Higgs boson pair (m_{hh}). The cross section of $gg \rightarrow hh$, after imposing the kinematic cuts, can be written as [56]

$$\sigma_{\text{cut}} = \int dm_{hh} \frac{d\sigma}{dm_{hh}} \mathcal{A}(m_{hh}) \quad (10)$$

where the efficiency function $\mathcal{A}(m_{hh})$ has been given in Refs. [56, 57], both for the 14 TeV LHC and the 100 TeV hadron collider. In Ref. [57], it is demonstrated that the results obtained from the analytic cut efficiency functions agree very well with other results with more detailed simulations [60].

The SM backgrounds for the process of $gg \rightarrow hh$ production include $b\bar{b}\gamma\gamma$, $c\bar{c}\gamma\gamma$, $b\bar{b}\gamma j$, $j\bar{j}\gamma\gamma$, $b\bar{b}jj$, $t\bar{t}(\geq 1\ell^\pm)$, $t\bar{t}\gamma$, $Z(\rightarrow b\bar{b})h(\rightarrow \gamma\gamma)$, $t\bar{t}h(\rightarrow \gamma\gamma)$ and $b\bar{b}h(\rightarrow \gamma\gamma)$, etc. At the 14 TeV LHC, with the integrated luminosity of $\mathcal{L} = 3 \text{ ab}^{-1}$ [68], and the 100 TeV hadron collider, with $\mathcal{L} = 30 \text{ ab}^{-1}$ [69], the signal (n_s) and background (n_b)

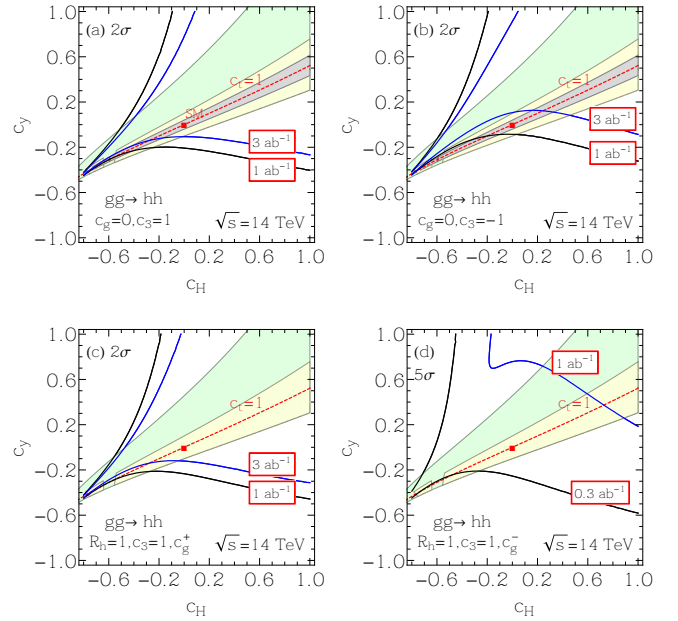


FIG. 4. The 2σ or 5σ discovery potential for $gg \rightarrow hh$ in the plane of c_H and c_y at the 14 TeV LHC. The green bands correspond to the constraints, at the 2σ C.L., from the measurements of $t\bar{t}h$ at the 13 TeV LHC. The gray and yellow bands represent the projected 2σ errors in the single Higgs production and $t\bar{t}h$ measurement at the HL-LHC, respectively. The red box denotes ($c_H = 0, c_y = 0$), while the red dashed line corresponds to $c_t = 1$. c_g^\pm refers to the sign choices “ \pm ” in Eq. (7) with R_h being fit from single Higgs production and decay data.

events in the SM are, respectively,

$$\begin{aligned} 14 \text{ TeV} : n_s &= 8.4, & n_b &= 47, \\ 100 \text{ TeV} : n_s &= 12061, & n_b &= 27118. \end{aligned} \quad (11)$$

With the event numbers listed above, the discovery potential for the signal process can be evaluated by using [70]

$$\mathcal{Z} = \sqrt{2 \left[(n_s + n_b) \log \frac{n_s + n_b}{n_b} - n_s \right]}. \quad (12)$$

In Figs. 4 and 5, we show the contours of discovery potential for $gg \rightarrow hh \rightarrow b\bar{b}\gamma\gamma$ at the 14 TeV LHC and the 100 TeV hadron collider, with various integrated luminosities. The 2σ and 5σ discovery potentials correspond to $\mathcal{Z} = 2$ and $\mathcal{Z} = 5$, respectively. As mentioned earlier, the signal strength R_h is measured with an accuracy of about 10%, and R_{hh} is not sensitive to the value of R_h (for $0.9 \leq R_h \leq 1.1$), we therefore take $R_h = 1$ as the benchmark to show the discovery potential in those figures.

Several comments are in order regarding the discovery potential of $gg \rightarrow hh$ with respect to the Wilson coefficients c_H and c_y . In Fig. 4, only the parameter space

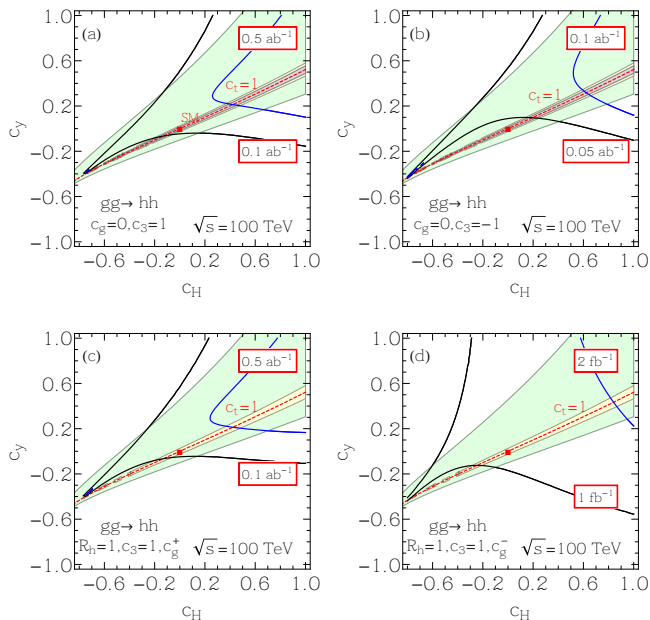


FIG. 5. The 5σ discovery potential for $gg \rightarrow hh$ in the plane of c_H and c_y at the 100 TeV hadron collider. The green bands correspond to the constraints, at the 2σ C.L., from the measurements of $t\bar{t}h$ at the 13 TeV LHC. The gray and yellow bands represent the projected 2σ errors in the $t\bar{t}h$ measurement at the 100 TeV hadron collider, with an integrated luminosity of 3 ab^{-1} at 2σ C.L., respectively. The red box denotes ($c_H = 0, c_y = 0$), while the red dashed line corresponds to $c_t = 1$. c_g^\pm refers to the sign choices “ \pm ” in Eq. (7) with R_h being fit from single Higgs production and decay data.

on the left of the curve, or below the curve, labeled by a specified integrated luminosity at the HL-LHC, can be reached at the 2σ or 5σ C.L.. For case (a), the SM point cannot be probed by measuring only the $gg \rightarrow hh$ production. A larger parameter space is reachable at 2σ C.L. for case (b), as compared to cases (a) and (c), due to the large enhancement of R_{hh} with negative c_3 . For case (d), with negative c_g , the Higgs pair production cross section can be enhanced by a factor of about 10, as compared to the SM value (cf. Fig. 3(f)). Consequently, with an integrated luminosity of 1 ab^{-1} at the HL-LHC, most of the considered parameter space (for $|c_H| < 1$ and $|c_y| < 1$) can already be reached at the 5σ C.L.. For comparison, in the same figure, we also show the constraints imposed by the projected 2σ errors in the single Higgs production and $t\bar{t}h$ measurement at the HL-LHC, with an integrated luminosity of 3 ab^{-1} . It amounts to $c_t = 1 \pm 0.02$ (single Higgs with $c_g = 0$) and $c_t = 1 \pm 0.05$ ($t\bar{t}h$ production) [71] which have included the statistical and experimental systematic uncertainties.

In Fig. 5, we see that the discovery potential for the $gg \rightarrow hh$ measurement is much improved at the 100 TeV hadron collider, for all the benchmark cases. The 5σ discovery significance can be easily reached. For cases (a)

and (c), large region of $c_y, c_H < 0.2$ can be discovered with the integrated luminosity of 0.5 ab^{-1} . For case (b), with negative c_3 , the region of $c_y, c_H < 0.5$ can be almost discovered with only 0.1 ab^{-1} . For case (d), with negative c_g , the currently allowed region can be explored with 2 fb^{-1} . For comparison, in the same figure, we also show the constraints imposed by the projected 2σ errors in the single Higgs production and $t\bar{t}h$ measurement at the 100 TeV hadron collider, with an integrated luminosity of 3 ab^{-1} . It amounts to $c_t = 1 \pm 0.0072$ (single Higgs production, with $c_g = 0$) and $c_t = 1 \pm 0.013$ ($t\bar{t}h$ production) [72, 73]. Note that both the statistical and systematic uncertainties are included in the single Higgs analysis, while only statistical error is discussed in $t\bar{t}h$ production. Here, we have scaled down the error in $t\bar{t}h$ measurement by the inverse of the square root of integrated luminosity.

To estimate the expected accuracy for measuring (c_H, c_y) with the Higgs pair production at the 14 TeV LHC and the 100 TeV hadron collider, respectively, we perform a log likelihood ratio test [70] for the hypothesis with non-zero c_H, c_y against the hypothesis with $c_H = c_y = 0$. The test ratio is defined as [70]

$$t = -2 \ln \frac{L(c_H, c_y)}{L(0, 0)} \quad (13)$$

where the likelihood function $L(c_H, c_y)$ is

$$L(c_H, c_y) = P(\text{data} | n_b + n_s(c_H, c_y)). \quad (14)$$

Here $P(k|\lambda)$ is the usual Poisson distribution function, $P(k|\lambda) = \lambda^k e^{-\lambda} / k!$. We assume the observed data is generated under the hypothesis with $c_H = c_y = 0$ [70, 74] and calculate the two-sided p -value. For convenience, we convert the p -value into the equivalent significance $Z = \Phi^{-1}(1 - 1/2p) = \sqrt{2} \text{Erf}^{-1}(1 - p)$ [70, 75], where Φ the cumulative distribution of the standard Gaussian and Erf is the error function. In our case, $Z = \sqrt{2[n_0 \ln \frac{n_0}{n_1} + (n_1 - n_0)]}$ with $n_0 = n_b + n_s(0, 0)$ and $n_1 = n_b + n_s(c_H, c_y)$. The discrimination between the hypothesis with arbitrary (c_H, c_y) and the hypothesis with $c_H = c_y = 0$ is shown in Figs. 6 and 7. The hypothesis with (c_H, c_y) outside of the blue bands is rejected at 1σ level for the HL-LHC and the 100 TeV hadron collider, respectively. After combining the measurements of single Higgs production (gray band) and $t\bar{t}h$ production (yellow band) at the HL-LHC, it is possible to differentiate c_H and c_y at the HL-LHC for cases (b) and (d), but it becomes challenging for cases (a) and (c), cf. Fig. 6. The situation will be much improved at the 100 TeV hadron collider, cf. Fig. 7. It is obvious that the Higgs pair production is more sensitive to c_y than to c_H . We find that at the 1σ C.L., the combined constraint from single Higgs production, $t\bar{t}h$ production and the Higgs pair production measurements, at the 100 TeV hadron collider with the

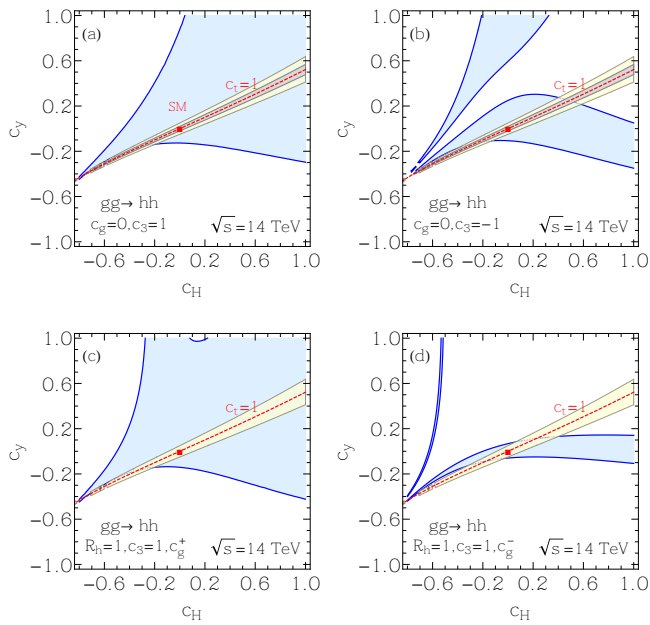


FIG. 6. Expected accuracy for measuring (c_H, c_y) with single Higgs production, $t\bar{t}h$ production and the Higgs pair production at the HL-LHC, with the integrated luminosity of 3 ab^{-1} . The gray, yellow and blue bands represent the 1σ constraint from the measurements of single Higgs production, $t\bar{t}h$ production and Higgs pair production at the HL-LHC, respectively. Both the statistical and experimental systematic uncertainties have been included in the single Higgs production and $t\bar{t}h$ production. The red box denotes $(c_H = 0, c_y = 0)$, while the red dashed line corresponds to $c_t = 1$.

integrated luminosity of 3 ab^{-1} , yields $-0.04 < c_y < 0$ and $-0.08 < c_H < 0.08$. To further constrain c_H , it is necessary to improve the measurement of $t\bar{t}h$ associated production. However, if the Higgs boson is a SM-like particle, c_H could be constrained by the hVV coupling measurement to $1\% \sim 2\%$ level [73].

Given the good sensitivity of differentiating c_H with c_y at the 100 TeV hadron collider, it is worthwhile clarifying the specific values of (c_H, c_y) , as induced by several generic classes of NP models [21, 23, 76]. Table I lists the Wilson coefficients c_H and c_y predicted by various NP models [21, 23, 76]. Both heavy scalars and vectors could contribute to c_H and c_y , while the additional heavy vector-like quarks (VLQs) could contribute to c_y and c_g . The sign of c_y is arbitrary in two Higgs doublet (2HDM) [21] and VLQ models [23]. Those NP models can be easily discriminated if they modify c_H or c_y by a sizable amount, cf. Fig. 7.

Conclusions. Both the Wilson coefficients c_H and c_y of dimension-six operators can contribute to the top quark Yukawa coupling simultaneously, thus their individual contributions cannot be separated with the measurement of $ht\bar{t}$ coupling alone. In this work, we demonstrate that c_H and c_y also contribute to the $t\bar{t}hh$ effective coupling

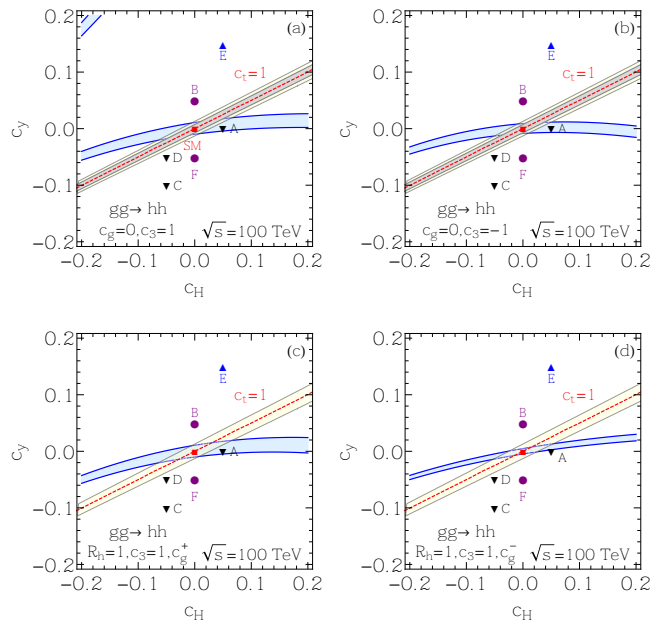


FIG. 7. Expected accuracy for measuring (c_H, c_y) with single Higgs production, $t\bar{t}h$ production and the Higgs pair production at the 100 TeV collider, with the integrated luminosity of 3 ab^{-1} . The gray, yellow and blue bands represent the 1σ constraint from the measurements of single Higgs production, $t\bar{t}h$ production and Higgs pair production at the 100 TeV collider, respectively. Both the statistical and experimental systematic uncertainties have been included in the single Higgs production. The red box denotes $(c_H = 0, c_y = 0)$, while the red dashed line corresponds to $c_t = 1$. For comparison, several benchmark points of NP models are also shown: A) singlet scalar, B) 2HDM or VLQs with $c_y > 0$, C) real triplet scalar, D) complex triplet scalar, E) vectors, F) 2HDM or VLQs with $c_y < 0$.

TABLE I. The Wilson coefficients c_H and c_y predicted by various NP models [21, 23, 76].

A) singlet scalar [21, 76]	B) 2HDM [21] or VLQs [23]
$c_H > 0, c_y = 0$	$c_H = 0, c_y > 0$
C) real triplet scalar [76]	D) complex triplet scalar [76]
$c_H = 2c_y < 0$	$c_H = c_y < 0$
E) vectors [76]	F) 2HDM [21] or VLQs [23]
$c_H = 3c_y > 0$	$c_H = 0, c_y < 0$

c_{2t} , whose information can be well extracted out from the Higgs pair production. Thus this process can be used to distinguish the effects of c_H and c_y at the 14 TeV LHC and the 100 TeV hadron collider. Regarding the discovery potential for the process $gg \rightarrow hh$, it shows that the 2σ confidence level is reachable for some parameter space at the 14 TeV LHC in general, and the sensitivity can be much improved at the 100 TeV hadron collider. Regrad-

ing the sensitivity of measuring c_t and c_H , we find it is challenging to differentiate c_H and c_y at the HL-LHC, except for some special scenarios. The situation will be much improved at the 100 TeV hadron collider. After combing the single Higgs production, $t\bar{t}h$ production at the 100 TeV hadron collider, the Higgs pair production can give a strong constraint on c_y regardless of the value c_H . The precise measurement of both c_H and c_y enable us to discriminate various new physics models.

Acknowledgements. We thank Kirtimaan A. Mohan for helpful discussions. The work of G. Li is supported by the MOST (Grant No. MOST 106-2112-M-002-003-MY3). L.-X. Xu is supported in part by the National Science Foundation of China under Grants No. 11635001, 11875072. B. Yan and C.-P. Yuan are supported by the U.S. National Science Foundation under Grant No. PHY-1719914. C.-P. Yuan is also grateful for the support from the Wu-Ki Tung endowed chair in particle physics.

* gangli@phys.ntu.edu.tw

† lingxiaoxu@pku.edu.cn

‡ yanbin1@msu.edu

§ yuan@pa.msu.edu

- [1] G. Degrossi, S. Di Vita, J. Elias-Miro, J. R. Espinosa, G. F. Giudice, G. Isidori, and A. Strumia, *JHEP* **08**, 098 (2012), 1205.6497.
- [2] F. Bezrukov and M. Shaposhnikov, *J. Exp. Theor. Phys.* **120**, 335 (2015), [*Zh. Eksp. Teor. Fiz.*147,389(2015)], 1411.1923.
- [3] S. P. Martin, pp. 1–98 (1997), [*Adv. Ser. Direct. High Energy Phys.*18,1(1998)], hep-ph/9709356.
- [4] R. Contino, in *Physics of the large and the small, TASI 09, proceedings of the Theoretical Advanced Study Institute in Elementary Particle Physics, Boulder, Colorado, USA, 1-26 June 2009* (2011), pp. 235–306, 1005.4269.
- [5] B. Bellazzini, C. Csaki, and J. Serra, *Eur. Phys. J.* **C74**, 2766 (2014), 1401.2457.
- [6] G. Panico and A. Wulzer, *Lect. Notes Phys.* **913**, pp.1 (2016), 1506.01961.
- [7] C. Csaki and P. Tanedo, in *Proceedings, 2013 European School of High-Energy Physics (ESHEP 2013): Paradfurdo, Hungary, June 5-18, 2013* (2015), pp. 169–268, 1602.04228.
- [8] M. Aaboud et al. (ATLAS), *Phys. Lett.* **B784**, 173 (2018), 1806.00425.
- [9] A. M. Sirunyan et al. (CMS), *Phys. Rev. Lett.* **120**, 231801 (2018), 1804.02610.
- [10] T. A. collaboration (ATLAS), *Tech. Rep. ATLAS-CONF-2018-031* (2018).
- [11] C. Collaboration (CMS), *Tech. Rep. CMS-PAS-HIG-17-031* (2018).
- [12] A. M. Sirunyan et al. (CMS), Submitted to: *Phys. Rev.* (2018), 1811.09696.
- [13] Q.-H. Cao, S.-L. Chen, and Y. Liu, *Phys. Rev.* **D95**, 053004 (2017), 1602.01934.
- [14] Q.-H. Cao, S.-L. Chen, Y. Liu, R. Zhang, and Y. Zhang (2019), 1901.04567.
- [15] A. Pomarol and F. Riva, *JHEP* **01**, 151 (2014), 1308.2803.
- [16] G. F. Giudice, C. Grojean, A. Pomarol, and R. Rattazzi, *JHEP* **06**, 045 (2007), hep-ph/0703164.
- [17] R. Contino, M. Ghezzi, C. Grojean, M. Muhlleitner, and M. Spira, *JHEP* **07**, 035 (2013), 1303.3876.
- [18] N. Craig, C. Englert, and M. McCullough, *Phys. Rev. Lett.* **111**, 121803 (2013), 1305.5251.
- [19] N. Craig, M. Farina, M. McCullough, and M. Perelstein, *JHEP* **03**, 146 (2015), 1411.0676.
- [20] S. Dawson and C. W. Murphy, *Phys. Rev.* **D96**, 015041 (2017), 1704.07851.
- [21] T. Corbett, A. Joglekar, H.-L. Li, and J.-H. Yu, *JHEP* **05**, 061 (2018), 1705.02551.
- [22] Q.-H. Cao, F. P. Huang, K.-P. Xie, and X. Zhang, *Chin. Phys.* **C42**, 023103 (2018), 1708.04737.
- [23] F. del Aguila, M. Perez-Victoria, and J. Santiago, *JHEP* **09**, 011 (2000), hep-ph/0007316.
- [24] C.-Y. Chen, S. Dawson, and E. Furlan, *Phys. Rev.* **D96**, 015006 (2017), 1703.06134.
- [25] Q.-H. Cao, L.-X. Xu, B. Yan, and S.-H. Zhu, *Phys. Lett.* **B789**, 233 (2019), 1810.07661.
- [26] E. W. N. Glover and J. J. van der Bij, *Nucl. Phys.* **B309**, 282 (1988).
- [27] U. Baur, T. Plehn, and D. L. Rainwater, *Phys. Rev.* **D68**, 033001 (2003), hep-ph/0304015.
- [28] U. Baur, T. Plehn, and D. L. Rainwater, *Phys. Rev.* **D69**, 053004 (2004), hep-ph/0310056.
- [29] M. J. Dolan, C. Englert, and M. Spannowsky, *JHEP* **10**, 112 (2012), 1206.5001.
- [30] J. Baglio, A. Djouadi, R. Grober, M. M. Muhlleitner, J. Quevillon, and M. Spira, *JHEP* **04**, 151 (2012), 1212.5581.
- [31] A. Papaefstathiou, L. L. Yang, and J. Zurita, *Phys. Rev.* **D87**, 011301 (2013), 1209.1489.
- [32] D. Y. Shao, C. S. Li, H. T. Li, and J. Wang, *JHEP* **07**, 169 (2013), 1301.1245.
- [33] F. Goertz, A. Papaefstathiou, L. L. Yang, and J. Zurita, *JHEP* **06**, 016 (2013), 1301.3492.
- [34] V. Barger, L. L. Everett, C. B. Jackson, and G. Shaughnessy, *Phys. Lett.* **B728**, 433 (2014), 1311.2931.
- [35] A. J. Barr, M. J. Dolan, C. Englert, and M. Spannowsky, *Phys. Lett.* **B728**, 308 (2014), 1309.6318.
- [36] D. E. Ferreira de Lima, A. Papaefstathiou, and M. Spannowsky, *JHEP* **08**, 030 (2014), 1404.7139.
- [37] Q. Li, Z. Li, Q.-S. Yan, and X. Zhao, *Phys. Rev.* **D92**, 014015 (2015), 1503.07611.
- [38] J. K. Behr, D. Bortoletto, J. A. Frost, N. P. Hartland, C. Issever, and J. Rojo, *Eur. Phys. J.* **C76**, 386 (2016), 1512.08928.
- [39] A. Alves, T. Ghosh, and K. Sinha, *Phys. Rev.* **D96**, 035022 (2017), 1704.07395.
- [40] A. Adhikary, S. Banerjee, R. K. Barman, B. Bhattacharjee, and S. Niyogi, *JHEP* **07**, 116 (2018), 1712.05346.
- [41] J. H. Kim, Y. Sakaki, and M. Son, *Phys. Rev.* **D98**, 015016 (2018), 1801.06093.
- [42] D. Goncalves, T. Han, F. Kling, T. Plehn, and M. Takeuchi, *Phys. Rev.* **D97**, 113004 (2018), 1802.04319.
- [43] J. Chang, K. Cheung, J. S. Lee, C.-T. Lu, and J. Park (2018), 1804.07130.
- [44] S. Borowka, C. Duhr, F. Maltoni, D. Pagani, A. Shivaji, and X. Zhao, Submitted to: *JHEP* (2018), 1811.12366.
- [45] S. Homiller and P. Meade, *JHEP* **03**, 055 (2019),

- 1811.02572.
- [46] J. H. Kim, K. Kong, K. T. Matchev, and M. Park, *Phys. Rev. Lett.* **122**, 091801 (2019), 1807.11498.
- [47] J. H. Kim, M. Kim, K. Kong, K. T. Matchev, and M. Park (2019), 1904.08549.
- [48] K. Agashe, R. Contino, and A. Pomarol, *Nucl. Phys.* **B719**, 165 (2005), hep-ph/0412089.
- [49] R. Contino, L. Da Rold, and A. Pomarol, *Phys. Rev.* **D75**, 055014 (2007), hep-ph/0612048.
- [50] N. Arkani-Hamed, A. G. Cohen, and H. Georgi, *Phys. Lett.* **B513**, 232 (2001), hep-ph/0105239.
- [51] N. Arkani-Hamed, A. G. Cohen, E. Katz, and A. E. Nelson, *JHEP* **07**, 034 (2002), hep-ph/0206021.
- [52] P. Huang, A. Joglekar, M. Li, and C. E. M. Wagner, *Phys. Rev.* **D97**, 075001 (2018), 1711.05743.
- [53] P. Basler, S. Dawson, C. Englert, and M. M?hleleitner (2018), 1812.03542.
- [54] K. S. Babu and S. Jana (2018), 1812.11943.
- [55] H.-L. Li, L.-X. Xu, J.-H. Yu, and S.-H. Zhu (2019), 1904.05359.
- [56] Q.-H. Cao, B. Yan, D.-M. Zhang, and H. Zhang, *Phys. Lett.* **B752**, 285 (2016), 1508.06512.
- [57] Q.-H. Cao, G. Li, B. Yan, D.-M. Zhang, and H. Zhang, *Phys. Rev.* **D96**, 095031 (2017), 1611.09336.
- [58] C.-R. Chen and I. Low, *Phys. Rev.* **D90**, 013018 (2014), 1405.7040.
- [59] F. Goertz, A. Papaefstathiou, L. L. Yang, and J. Zurita, *JHEP* **04**, 167 (2015), 1410.3471.
- [60] A. Azatov, R. Contino, G. Panico, and M. Son, *Phys. Rev.* **D92**, 035001 (2015), 1502.00539.
- [61] S. Dawson, A. Ismail, and I. Low, *Phys. Rev.* **D91**, 115008 (2015), 1504.05596.
- [62] T. Plehn, M. Spira, and P. M. Zerwas, *Nucl. Phys.* **B479**, 46 (1996), [Erratum: *Nucl. Phys.*B531,655(1998)], hep-ph/9603205.
- [63] S. Dawson, E. Furlan, and I. Lewis, *Phys. Rev.* **D87**, 014007 (2013), 1210.6663.
- [64] T. Plehn, *Lect. Notes Phys.* **844**, 1 (2012), 0910.4182.
- [65] T. A. collaboration (ATLAS), *Tech. Rep. ATLAS-CONF-2018-043* (2018).
- [66] A. M. Sirunyan et al. (CMS), Submitted to: *Phys. Rev. Lett.* (2018), 1811.09689.
- [67] Q.-H. Cao, Y. Liu, and B. Yan, *Phys. Rev.* **D95**, 073006 (2017), 1511.03311.
- [68] *Tech. Rep. ATL-PHYS-PUB-2014-019*, CERN, Geneva (2014), URL <https://cds.cern.ch/record/1956733>.
- [69] R. Contino et al., *CERN Yellow Report* pp. 255–440 (2017), 1606.09408.
- [70] G. Cowan, K. Cranmer, E. Gross, and O. Vitells, *Eur. Phys. J.* **C71**, 1554 (2011), [Erratum: *Eur. Phys. J.*C73,2501(2013)], 1007.1727.
- [71] *Tech. Rep. ATL-PHYS-PUB-2014-016*, CERN, Geneva (2014), URL <http://cds.cern.ch/record/1956710>.
- [72] M. L. Mangano, T. Plehn, P. Reimitz, T. Schell, and H.-S. Shao, *J. Phys.* **G43**, 035001 (2016), 1507.08169.
- [73] M. Mangano, P. Azzi, M. Benedikt, A. Blondel, D. A. Britzger, A. Dainese, M. Dam, J. de Blas, D. Enterria, O. Fischer, et al., *Tech. Rep. CERN-ACC-2018-0056*, CERN, Geneva (2018), submitted for publication to *Eur. Phys. J. C.*, URL <https://cds.cern.ch/record/2651294>.
- [74] N. Kumar and S. P. Martin, *Phys. Rev.* **D92**, 115018 (2015), 1510.03456.
- [75] M. Tanabashi et al. (Particle Data Group), *Phys. Rev.* **D98**, 030001 (2018).
- [76] I. Low, R. Rattazzi, and A. Vichi, *JHEP* **04**, 126 (2010), 0907.5413.